Molecular dynamics study of rhodamine 6G diffusion at n-decane–water interfaces

Piotr Popov, Leo Steinkerchner, and Elizabeth K. Mann

Molecular dynamics study of rhodamine 6G diffusion at *n*-decane/water interfaces.

Piotr Popov[1], Leo Steinkerchner[1,2], Elizabeth K. Mann[1]

[1]Physics Department, Kent State University, Kent, Ohio, USA, 44242
[2]Wadsworth High School, Wadsworth, Ohio, USA, 44281

Abstract: Two-dimensional diffusion of a rhodamine 6G fluorescent tracer molecule at the *n*-decane/water interface was studied with all-atom molecular dynamics (MD) simulations. In agreement with experimental data, we find increased mobility of the tracer at the *n*-decane/water interfaces in comparison to its mobility in bulk water. Orientational ordering of water and *n*-decane molecules near the interface is observed, and may change the interfacial viscosity as suggested to explain the experimental data. However, the restricted rotational motion of the rhodamine molecule at the interface suggests that Saffman-Delbrück model may be a more appropriate approximation of rhodamine diffusion at *n*-decane/water interfaces, and, without any decrease in interfacial viscosity, suggests faster diffusion consistent with both experimental and simulation values.

PACS number(s): 68.05.-n, 47.90.+a, 02.70.-c

Introduction

The dynamics of adsorbed molecules at liquid/liquid interfaces are critical to two-dimensional soft-matter systems, with practical applications in nanotechnology, microfluidics, biosensors and drug delivery [1–3]. Important biological examples include diffusion-limited processes of lipids [4,5] and membrane-embedded proteins [6] that play important roles in signal transduction at cell interfaces [7].

1

The tiny interfacial thickness, usually less than ten nanometers, limits experimental techniques. Many of the most important ones use amphiphilic fluorescent tracers to directly probe motion at and around interfaces. For example, to measure diffusion coefficients of insoluble surfactant monolayers, Jeong and coworkers developed the technique of fluorescence recovery after merging a surfactant-covered droplet [8]. Negishi and colleagues observed the diffusion of fluorescent phospholipids at the oil/water interfaces of cell-sized microdroplets and concluded that lipid mobility is primarily affected by the viscosity of the oil phase [9]. Walder et al. used fluorescent recovery after photobleaching (FRAP) microscopy to study diffusion rates of phospholipids at oil/water interfaces and suggested that at high oil viscosity the Stokes-Einstein dynamics may switch to desorption activated ("hopping") dynamics [10]. In another study, Kastantin et al. looked at heterogeneous interfacial behavior (diffusion, adsorption/desorption) by tracking single fluorescent molecules [11].

This paper presents a molecular dynamics simulation study of rhodamine 6G fluorescent tracer at the *n*-decane/water interface. Our work was inspired by experimental observations by Wang et al. [12], who used fluorescent correlation spectroscopy (FCS) to study diffusion of water-soluble fluorophores of different sizes at alkane/water interfaces. A particularly intriguing observation was made for the diffusion of smaller fluorescent molecules at the *n*-decane/water interface. At room temperature (~22°C) the viscosities of *n*-decane and water become very close to each other. Therefore, a naïve prediction suggests that the diffusion coefficient of a small molecule incorporated at the *n*-decane/water interface would be the same as that in bulk water. Wang and colleagues found that fluorophores of large hydrodynamic radius (~4 nm) indeed exhibit the same

mobilities in both cases, but the diffusion constants for the smaller perylene dye PDI (~1 nm) and for rhodamine 6G (~0.6 nm) *increased* at the *n*-decane/water interface, by factors of 1.15 and 1.4 respectively. If the R6G molecule can be treated in the same spherical approximation in both environments, in bulk water and at the oil/water interfaces, then the increased mobility of the R6G at the interface must, as suggested by Wang et al. [12], be due to reduced effective interfacial viscosity, perhaps because of depletion within the interfacial layer.

Our work offers atomic-level insight into the interfacial diffusion behavior of the smallest tracer rhodamine 6G (R6G) through atomistic molecular dynamics simulations. In agreement with Wang et al. [12], we find increased mobility of the tracer at the *n*-decane/water interface in comparison to its value in bulk water. We also observe that the orientation of R6G is severely restricted at the interface, and suggest that it might be more appropriate to approximate the rhodamine molecule as a hydrodynamic cylinder in the interfacial environment rather than the simpler hydrodynamic sphere appropriate in bulk. This difference alone may explain much of the contrast in diffusion constants.

Simulation methods

Molecular dynamics parameters

All-atom molecular dynamics (MD) simulations were used to investigate the mobility of a single rhodamine 6G (R6G) tracer molecule (see Figure 1) at the *n*-decane/water interface.

The atomic interactions were defined by a recent version of the Optimized Potentials for Liquid Systems (OPLS) force field [13], with new and improved

parameters [14,15]. The biphenyl-like dihedrals in R6G, which are not parameterized in the standard OPLS force field, were parameterized as described in Smith et al. [16]. For most of the results presented, the parameterization of *n*-decane molecules was adopted from the work of Siu et al, who developed an improved force field L-OPLS for long hydrocarbons [17], but some results are presented using the OPLS force fields for comparison. The assembly and parameterization of the R6G molecule was guided by the work of Vaiana et al. [18], where the CHARMM force field was used. A cut-off length of 1 nm was used for the Van der Waals and Coulombic short-range interactions. The long-range interactions were evaluated via the Particle Mesh Ewald method [19] with cubic interpolation. The simulations were carried out at constant number of molecules, pressure and temperature (NPT ensemble). The temperature in all simulations was maintained at 295.15 K (22°C, the temperature for the comparable experiments in Ref. [12]), and was coupled to the water and *n*-decane phases separately via the Nosé-Hoover thermostat [20] with a 0.2 ps coupling time constant. No separate temperature coupling to the R6G molecule was used, because the number of degrees of freedom of a single molecule is too small to justify a dedicated thermostat. The R6G molecule receives heat directly from the water and *n*-decane phases. The pressure was maintained at 1.01325 bar (1 Atm) by using the Parrinello-Rahman barostat [21] with a 1 ps coupling time constant. In simulations of R6G in bulk water, the box was allowed to scale in all three directions. In simulations of R6G with water and *n*-decane, the box was allowed to scale only in z-axis direction, to maintain a stable interface. The molecular dynamics time step was 2 fs. Coordinates for each atom were saved every 5000 steps. We used the GROMACS software package [22–24] for MD simulations, Avogadro Molecule Editor [25] for assembling individual

molecules, Packmol [26,27] for molecular packing of initial MD starting points, and VMD[TM] for visualizing [28] and rendering MD scenes [29]. The simulations were carried out with computational resources from the Ohio Supercomputer Center.
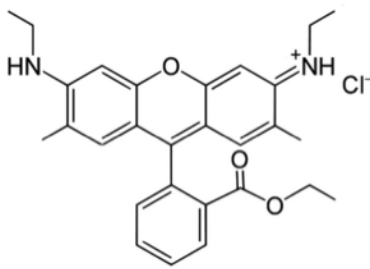

Figure 1: Chemical structure of R6G. Not shown: hydrogen atoms bonded to carbons.

The R6G was simulated in two different environments: in bulk water and at the *n*-decane/water interface.

The R6G molecule is fully ionized over a broad range of pH values around pH=7 [30,31]. For this reason, the R6G molecule in our simulations in water or at an interface has a charge of +1, directly enforced by making one of the nitrogen atoms positively charged. Its chlorine counter-ion of charge -1 is placed in the aqueous phase. Thus, the total system charge is 0. The chlorine ion diffuses independently of the rhodamine. To further test for an effect of the chlorine ion, we removed it from the system; the diffusion constant was unchanged, both when suppressing and maintaining the rhodamine charge.

In these simulations, periodic boundary conditions were applied for x, y and z dimensions. Steepest descent energy minimizations were performed on the initial configurations. Then, 10 ns of equilibrations were run before the actual production molecular dynamics simulations.

Effect of finite system size

Periodic boundary conditions (PBC) are used to model a large (infinite) system by explicitly modeling only a small part of it, a simulation unit cell of size L. Long-range electrostatic and hydrodynamic interactions may lead to significant deviations when the PBC method is applied. Yeh et al. demonstrated that properties such as density and liquid viscosity show no significant system-size dependence, while the diffusion coefficient depends on the system size [32]:

$$D_{PBC} = D - \xi \frac{k_B T}{6\pi \cdot \eta \cdot L} \qquad (1)$$

where $\xi \approx 2.837297$ is the PBC correction coefficient, D is the diffusion coefficient of a particle in an infinite system and D_{PBC} is the diffusion coefficient of a particle in a cubic simulation box of size L. Yeh et al. suggested that hydrodynamic interactions are primarily responsible for this effect, because the fluid velocity field $\vec{v}(\vec{r})$ generated by a point force $\vec{F}$ decays slowly (inversely proportional to distance r) [32].

Model validation.

Validation of water model

Figure 2 shows the simulation box filled with 4121 water molecules and a single R6G fluorophore. The water molecule is represented by the SPC/E model [33]. This 3-site water model was found to provide the best experimental agreement [34] and simulation efficiency. The self-diffusion coefficient was found to be, from a 100 ns long simulation corrected using Equation 1, $D_{w/self}=(2.384\pm0.017)\times10^{-5}$ cm^2/s, which agrees well with measurements ($D_{w/self\ exp}=(2.2990\pm0.0023)\times10^{-5}$ cm^2/s [35]). The viscosity of

SPC/E water was found to be $\eta_{SPC/E}$=0.940±0.061 cP (using the periodic perturbation method; see ref. [36] for detailed derivation of the viscosity value and its uncertainty) and is in good agreement with the experimental value of η_{exp}=0.9548 cP [37].
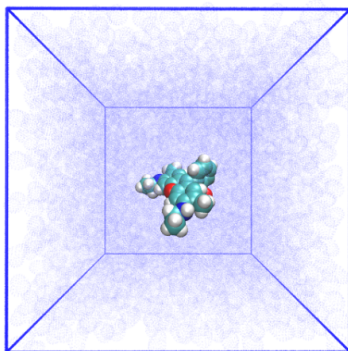

Figure 2: (Color online) R6G molecule centered in a box of SPC/E water. The size of the box is ~5×5×5 nm^3 (volume is not conserved in the NPT ensemble)

Validation of R6G diffusion model in bulk water

We conducted a 100 ns long simulation of R6G in water to compare the simulation R6G diffusion coefficient with the experimental one. No simulation was done for R6G in bulk *n*-decane, because we found no comparable experimental data. The diffusion coefficient can be obtained by calculating the mean squared displacement (MSD) as a function of time:

$$\langle r^2 \rangle = 2 \cdot d \cdot D_{PBC} \cdot t \qquad (2)$$

Where $\langle r^2 \rangle$ is the MSD, *d* is the number of dimensions, D_{PBC} is the diffusion coefficient for a particular box size and *t* is the time. The bracket symbol $\langle\,\rangle$ indicates the ensemble average. The obtained value is then corrected by using Equation 1 to obtain the diffusion coefficient D for an infinite system. We simulate a single trajectory of R6G's center of mass (COM), and in place of an ensemble average for MSD, sample a large number of

shorter subtrajectories and average over all of them. This treatment assumes that the Brownian motion is a Markov process [38], which means that the next "step" of a diffusing object does not depend on its previous "step" (or past trajectory). The diffusion time must be long compared to the time scale at which velocity (COM velocity) autocorrelation vanishes. From our simulations we obtained that velocity autocorrelation goes to zero within ~2 ps (MD integration step is 2 fs). The shortest subtrajectory we considered in this study is ~500 longer (~1 ns). In Figure 3a we show the diffusion lengths $\Delta l = \sqrt{\langle r(\Delta t)^2 \rangle}$ of R6G that are obtained for increasing time intervals $\Delta\tau$ of Brownian motion. Each point in Figure 3a was generated from a sample of 10^5 subtrajectories drawn randomly from the 100 ns trajectory. The subtrajectories may overlap with each other.

Figure 3b presents the diffusion coefficients calculated for different diffusion time intervals. The diffusion coefficient values are system-size corrected using Equation 1. The uncertainty bars around each point are the standard errors of the estimated diffusion coefficient [39] obtained from linear fitting to Equation 2. The bulk diffusion coefficients are in very good agreement with experimental findings $D_{exp} = 3.8 \times 10^{-6}$ cm^2/s [12,40,41].
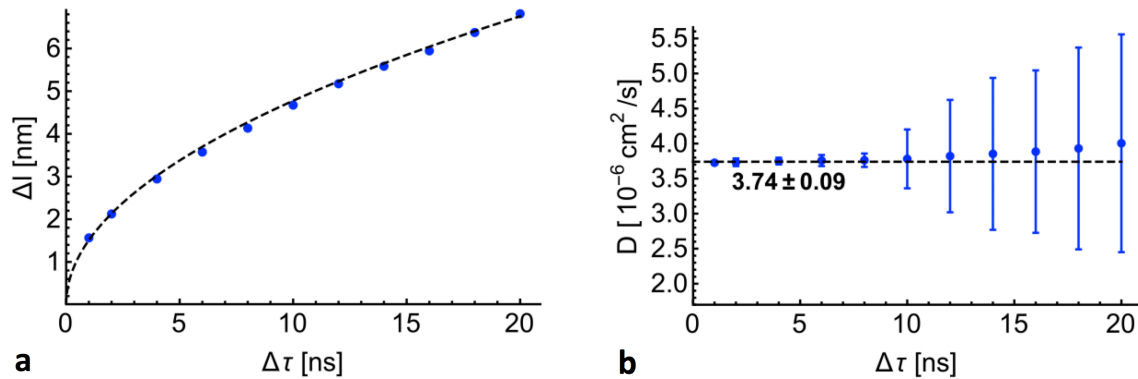

Figure 3: (Color online) Diffusion distance and diffusion coefficient of R6G in bulk water as functions of subtrajectory time: (a) Diffusion length: blue dots calculated from a

100 ns simulation in a ~5×5×5 nm³ box, corrected for finite size; dashed curve generated from theoretical expression using the diffusion coefficient as obtained from experiment $D=3.8\times10^{-6}$ cm²/s [40]. (b) Diffusion constant: blue dots calculated from 100 ns simulation, corrected for finite size; dashed curve is a linear weighted fit to a constant.

The hydrodynamic radius R_H is defined by the Stokes-Einstein relation: $D=k_BT/6\pi\eta R_H$, where k_BT is the Boltzman's constant times absolute temperature and η is the viscosity of the solvent. Using the diffusion coefficient from our simulation $D=(3.74\pm0.15)\times10^{-6}$ cm²/s, we calculate the hydrodynamic radius $R_H=0.605\pm0.025$ nm, which is in very good agreement with previous experimental values: 0.589 nm at 22°C [40] and 0.6 nm at 22°C [12].

Validation of n-decane parameterization

The *n*-decane molecule was parameterized within the all-atom L-OPLS definitions [17], rather than the more standard OPLS force field. Siu and colleagues demonstrated [17] that the viscosities of longer hydrocarbons are better-reproduced using the L-OPLS force field. For example, we find, applying the periodic perturbation method [36], that the viscosity of *n*-decane at 22°C in OPLS is $\eta_{OPLS}=1.345\pm0.023$ cP and in L-OPLS $\eta_{L\text{-}OPLS}=1.098\pm0.048$ cP. The latter value is closer to the experimentally measured $\eta_{exp}=0.9$ cP [12].

Results: simulations at the *n*-decane/water interface

Characterization of the interface: density profiles

The properties of the *n*-decane/water interface were characterized by using one of the three interfacial simulations that we conducted in this study. In Figure 4a we show the R6G fluorophore placed at the oil-water interface in a simulation box which has a volume of $\sim 7\times7\times6.5$ nm^3. As we will show later, to obtain a diffusion coefficient for R6G at the interface that is independent of the simulation box size, one needs to perform multiple simulations with varying box volume.

The density distributions across the box in z direction of the *n*-decane/water system are shown in Figure 4b. The calculated average densities are in good agreement with experimental measurements: for water $\rho=992\pm1$ kg/m^3 (experimentally $\rho=997.77$ kg/m^3 at 22°C [37]); for *n*-decane $\rho=732\pm5$ kg/m^3 (experimentally $\rho=728.86$ kg/m^3 at 22°C [42]).
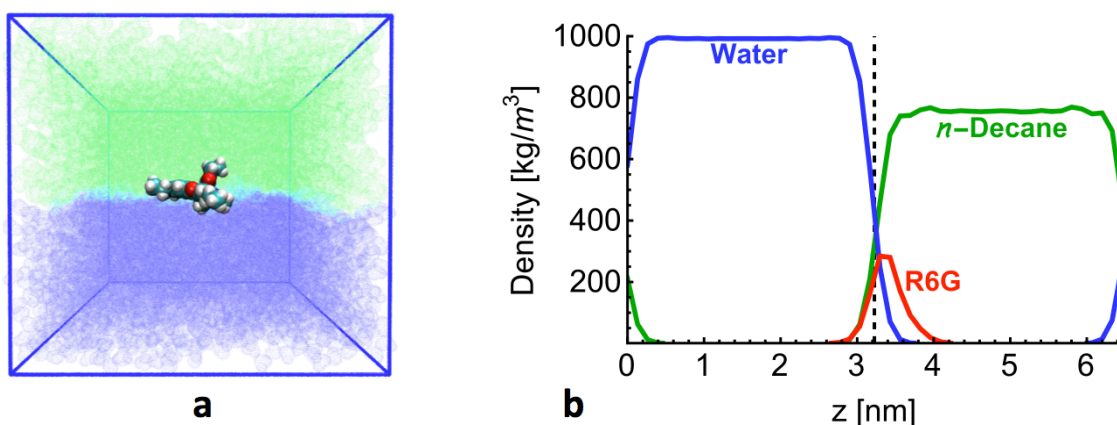

Figure 4: (Color online) R6G molecule at the *n*-decane/water interface: (a) R6G representation in the simulation box. Water shown in blue below R6G and *n*-decane

shown in green above R6G. Box size: ~7×7×6.5 nm³ (volume not conserved in NPT ensemble). (b) Partial densities across the box in z-axis direction: water partial density in blue; *n*-decane partial density in green; R6G partial density in red. The values of partial density of R6G were multiplied by a factor of 10 for clarity on graph. Vertical dashed line shows the position of the *n*-decane/water interface z=3.225 nm.

The interface is located in a range from z=3.20 nm to z=3.25 nm as determined by both the "half-density" method [43] and the "Gibbs dividing plane" method [44], for both water and decane.

Figure 4b shows the z-coordinate of R6G's center of mass (COM) $z_{COM(R6G)}$=3.35±0.05 nm (most probable position). The position of the R6G is thus slightly above the interface (Δz≈0.1 nm), so that R6G is mostly submerged into the *n*-decane phase.

Characterization of the interface: orientation of n-decane molecules

The behavior of a diffusing molecule depends on the state (orientation, alignment, etc.) of the surrounding molecules. Here we compare the orientations of molecules near the interface with those that are located in the bulk phases. This orientational analysis can offer useful insight into the influence of the interface on the diffusing molecule.

The orientation preference of *n*-decane molecules near the interface is expressed by the order parameter $S_{zz} = \frac{1}{2} \langle 3\cos^2\theta_i - 1 \rangle$, where θ_i is the angle between ith molecular axis and the interface normal (z-axis). The molecular axis is defined as the vector from C_{n-1} to C_{n+1} (C denotes a carbon atom). The triangular brackets here $\langle \rangle$ indicate the ensemble and time average. The order parameter can vary between 1 (perfect

order along the interface normal) and -1/2 (perfect order perpendicular to the interface normal) with a value of 0 in case of total disorder (isotropic state).

Figure 5a shows the order parameter variation across the *n*-decane phase in the z direction. In the bulk phase the order parameter is $S_{zz} \approx 0$, indicating no preferred orientation. The *n*-decane molecules in direct contact with water tend to orient laterally with respect to the interface plane where the order parameter is $S_{zz} \approx -0.2$. The orientational persistence length (the distance over which the observed order parameter decays by a factor of *e* from its extremum near the interface) of *n*-decane is 0.465 nm (see Figure 5a).

Characterization of the interface: orientation of water molecules

The orientational order of water molecules is defined as the average cosine of the angle θ between the unit vector of the dipole $\hat{\mu}$ and the unit vector normal to the interface $\hat{n}_z$ [45]: $\langle \cos\theta \rangle = \langle \hat{\mu} \cdot \hat{n}_z \rangle$. The triangular brackets $\langle\,\rangle$ indicate the ensemble average. Figure 5b shows the average dipole orientation of water molecules near the interface (position indicated with a dashed vertical line). The graph suggests that the water dipole moment orients near the interface. The orientational persistence length of water near a hydrophobic interface is 0.440 nm and is in good agreement with previous studies [45,46]. As is suggested by van Buuren et al. [46], at the interface the number of neighboring water molecules available for hydrogen bonding is smaller, and the water molecules orient themselves to create more possibilities for hydrogen bonding.
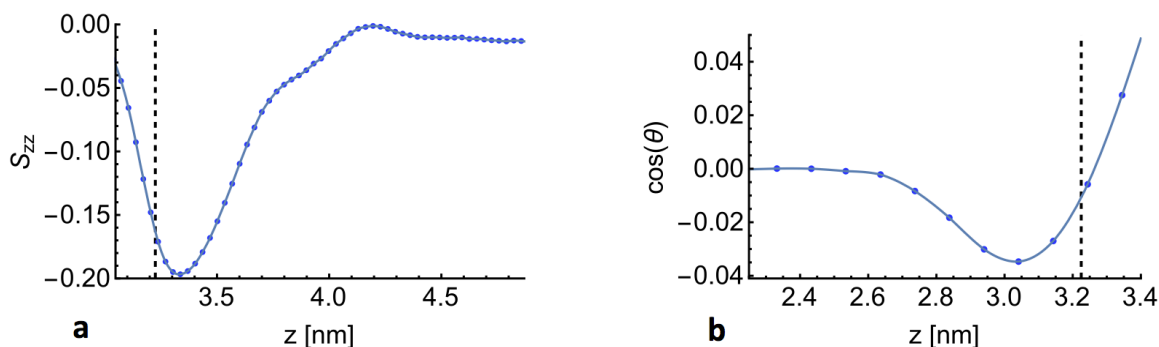
Figure 5: (Color online) Molecular orientations of *n*-decane and water at the interface: (a) Order parameter of *n*-decane as a function of the box length in z direction. (b) Orientation of water molecules as a function of the box length in z direction. Vertical dashed lines show the position of the *n*-decane/water interface z=3.225 nm. Lines are to guide the eye.

Rhodamine orientation at the interface

The orientation of the rhodamine in the x-y plane was random, as expected, but its orientation with respect to the z axis was well-defined. Figure 6a shows the orientation of ethylaniline moiety, given by the angle, α, between the arrow between its end points, illustrated in the figure inset, and the z-axis. The relatively large width of the distribution is due to a combination of the flexibility of the ethylanyline moiety and the roughness of the interface. Figure 6b shows the orientation of xanthene moiety, through the angle between the vector normal of the plane that contains the three rings, as shown in the molecular model in the inset to the graph, and the z-axis. The much narrower width of the orientation distribution of the stiff xanthene moiety is due to the roughness of the interface and any molecular pitching with respect to the surface, without the flexibility contribution.
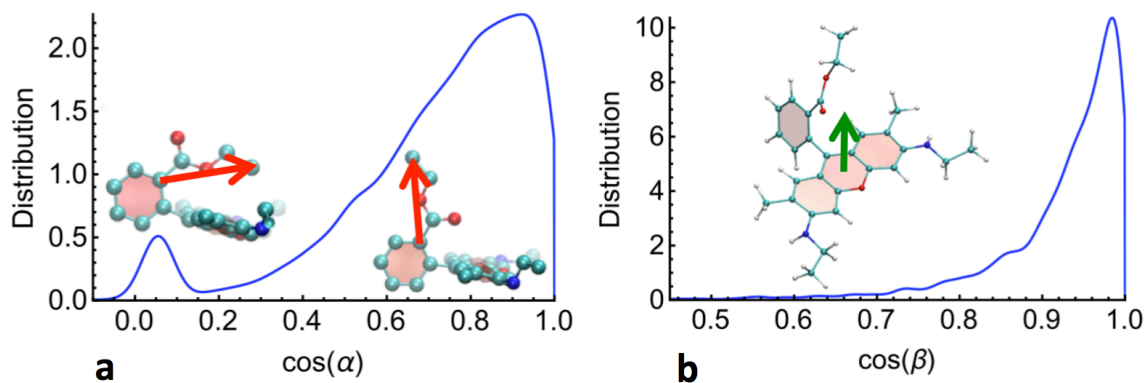
Figure 6: (Color online) Orientations of R6G moieties: (a) The orientation $\cos(\alpha)$ of ethylaniline moiety is towards the *n*-decane phase (positive direction of z-axis). (b) The orientation $\cos(\beta)$ of xanthene moiety. The molecular insets give typical orientations corresponding to the peaks, and define the orientations, given by the angle between the arrows in the inset figures and the z axis. Note that R6G never flips at the interface during the simulation.
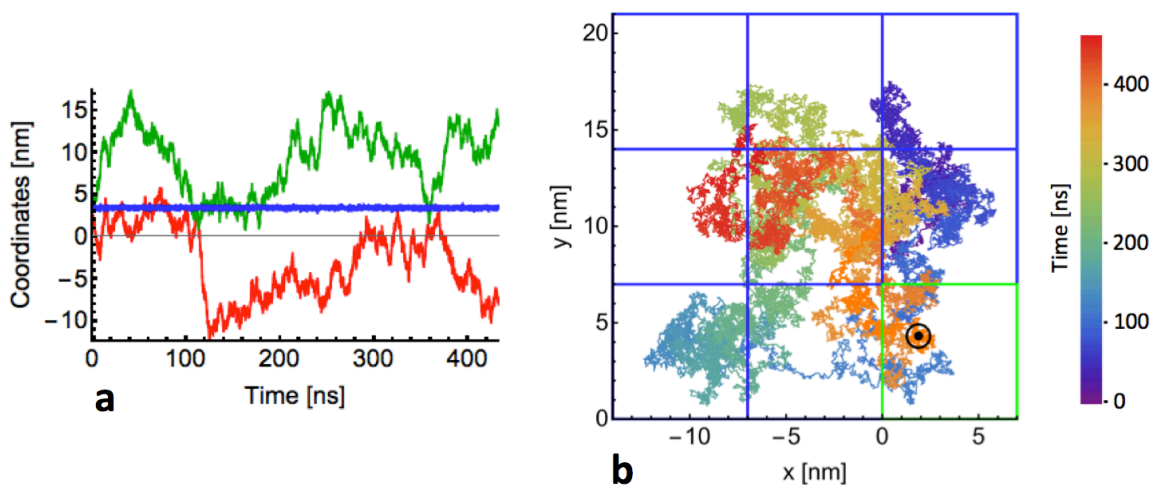
Diffusion of R6G at the interface.

Figure 7: (Color online) (a) Coordinates of R6G center of mass: red and green jagged trajectories for x and y coordinates, respectively; blue flat trajectory for z coordinate. Simulation time is 433 ns. (b) x-y coordinate map for R6G. Squares represent the

periodic images of the interface. The green square represents the starting image. The black dot and black circle represent the initial location and hydrodynamic size of the rhodamine molecule, respectively. The time is color-coded.

As expected, the RG6 molecule diffuses parallel to the surface (Figure 7a,b) while remaining tightly confined there (Figure 7a.) The z-coordinate (of the center of mass) of the rhodamine is $z=3.36\pm0.11$ nm, while the maximum vertical displacement is ±0.57 nm around the average position. The vertical displacements are associated with the roughness of the interface [47].

To calculate the diffusion coefficient of R6G at the *n*-decane/water interface, we performed three simulations varying the system size. This variation is needed to correct for periodic boundary conditions; previous results, summarized in Equation 1, were obtained for a diffusing molecule in the bulk of a liquid [32], while we are interested in the diffusion at a liquid/liquid interface. The system sizes and resulting diffusion constants are found in Table 1.

Figure 8a presents the diffusion coefficient values obtained from simulations of different box sizes. Equation [1], from ref. [32], cannot be used directly, as it was developed for a uniform liquid in a square box. We expect, however, that the linear relationship between the calculated diffusion constant and 1/L holds for this new system, with an interface and a box which is not quite square (with L the average box length.) We thus find the true diffusion constant by extrapolating the box dimensions to infinity; the limited practical range of system size limits the accuracy of the extrapolation, but we see a clear trend (see Figure 8b).
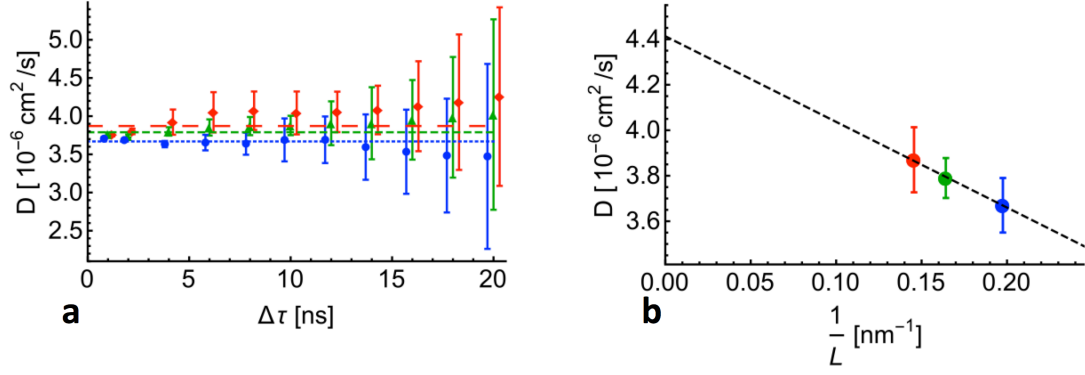
Figure 8: (Color online) Diffusion coefficients of R6G at *n*-decane/water interfaces in varying simulation boxe sizes: (a) Blue circles with uncertainty bars are diffusion coefficients of R6G in the small box (~5.2×5.2×4.9 nm^3) and the blue horizontal short-dashed line is the linear fit to a constant; green triangles with uncertainty bars are diffusion coefficients of R6G in the medium box (~6.2×6.2×5.8 nm^3) and the green horizontal medium-dashed line is the linear fit to a constant; red diamonds with uncertainty bars are diffusion coefficients of R6G in the large box (~7×7×6.5 nm^3) and the red horizontal long-dashed line is the linear fit to a constant; The blue and red data points are slightly x-axis-displaced to avoid the overlap of the uncertainty bars. (b) Diffusion coefficients of R6G as a function of the inverse length 1/L of the simulation box, where L is the average length of the box. The dashed line is a linear fit extrapolation to a box of infinite size D(1/L → 0). Fit parameters are given in Table 1.

The extrapolated value of R6G's diffusion coefficient is $D_{L\text{-OPLS}}=(4.4\pm0.1)\times10^{-6}$ cm^2/s can be now compared to the experimentally measured value of $D_{exp}=5.3\times10^{-6}$ cm^2/s [12]. The simulation value (from extrapolation) is lower than the experimental value, because in the simulation the viscosity of *n*-decane is higher (See Table 1) than in reality ($\eta_{exp}=0.9$ cP). Since the R6G molecule is mostly embedded into the *n*-decane

phase (see Figure 4), the resulting diffusion coefficient depends mostly on the value of the n-decane viscosity rather than on that for water. To estimate the correction for the high simulation value of the n-decane viscosity, we multiply D_{L-OPLS} by η_{L-OPLS}/η_{exp} to obtain $D_{corrected}=(5.4\pm0.1)\times10^{-6}$ cm^2/s, which is very close to the experimental value $D_{exp}=5.3\times10^{-6}$ cm^2/s [12]. The corrected value is also consistent with the diffusion constant extrapolated to the experimental n-decane viscosity from the diffusion constants determined with the two different force fields, which also gave different n-decane viscosities (see Table 1).

Table 1: Simulation values for n-decane viscosity and for diffusion coefficients at the n-decane/water interface, with different box sizes and different interatomic potential parameterizations. The infinite box values are extrapolated from the finite size box in the L-OPLS data, and increased by the same fraction for the OPLS data. See text for the viscosity corrections applied to the diffusion constants given in the last line.

Conditions	L-OPLS [17]					OPLS [13]	
	Size [nm^3]	N_{decane}	N_{water}	n-Decane Viscosity [cP]	$D\times10^{-6}$ [cm^2/s]	n-Decane Viscosity [cP]	$D\times10^{-6}$ [cm^2/s]
Small box	5.2×5.2×4.9	200	2117		3.67±0.12		-
Medium box	6.2×6.2×5.8	350	3703	1.098 ±0.048	3.79±0.09	1.345 ±0.023	-
Large box	7×7×6.5	500	5289		3.87±0.14		3.30±0.09
∞ box	∞	∞	∞		4.4±0.1		3.75±0.1*
Viscosity corrections					5.4±0.1		4.9±0.1*

* Assumes the same box size correction factor as for L-OPLS

Discussion and conclusions

Consistent with the experimental study [12], this MD simulation study finds a diffusion constant for rhodamine 6G significantly larger at the n-decane/water interface than in bulk water: in the simulation, the diffusion constant was 16% larger, compared to

39% larger in the experiment. As discussed above, most of the discrepancy is probably due to the simulation overestimate of the alkane viscosity.

This all-atom MD simulation enables a molecular-level interpretation of the higher interfacial diffusion constant. As shown in Figure 5, the water and *n*-decane molecules become oriented near the interface. This interfacial ordering could in principle change the diffusion coefficient as suggested by Wang and coworkers [12]. However, the almost fixed orientation of the R6G molecule (see Figure 6) suggests another explanation.

In the experimental study by Wang and coworkers [12], the R6G molecule is approximated as a sphere of constant radius in both environments: in bulk water and at the oil/water interfaces. This assumption leads directly to the conclusion that the increased mobility of the R6G at the interface is solely due to a reduced interfacial viscosity, suggesting a depletion interfacial layer. The simulations do not put in evidence such a depletion layer.

We suggest that the restricted rotational behavior of the rhodamine at oil/water interfaces is also very important. The restricted rotational motion (see Figure 6) forces the xanthene moiety to lie flat at the interface, which means that the molecule can no longer be approximated as a sphere; a cylindrical approximation may be more appropriate.

The motion of R6G molecule at the oil/water interface resembles the motion of proteins or lipid rafts within a lipid bilayer, for which an exact solution was obtained by Hughes et al.[29]. Later, Petrov et al. [49] developed a simple, accurate analytical approximation to the Hughes et al. model:

$$D_{int} = \frac{k_B T}{4\pi \cdot \eta_{int} \cdot h} \cdot \frac{\left(1 - \frac{\epsilon^2}{2}\right)\log\frac{2}{\epsilon} + \frac{4\epsilon}{\pi} - \gamma}{1 - \frac{\epsilon^2}{\pi}\log\frac{2}{\epsilon} + \frac{c_1 \cdot e^{b_1}}{1 + c_2 \cdot e^{b_2}}} \tag{3}$$

where η_{int} is the interfacial viscosity, $\gamma = 0.577$ is Euler-Mascheroni constant, $b_1 = 2.74819$, $b_2 = 0.51465$, $c_1 = 0.73761$, and $c_2 = 0.52119$ are fitting parameters and $\epsilon = \frac{R_{CH}}{h} \frac{(\eta_{water} + \eta_{decane})}{\eta_{int}}$ is the Saffman-Delbrück coefficient [50]. R_{CH} and h are the hydrodynamic cylindrical radius and height, respectively.

The effective cylindrical dimensions R_{CH} and h can be estimated from Equation 3. First we assume, to test the plausibility of the increased diffusion constant without reduced interfacial viscosity, that $\eta_{int} = \eta_{decane} \approx \eta_{water}$ (using experimental viscosities), and that the spherical and cylindrical effective molecular volumes should match: $V_C = V_S$, where $V_S = \frac{4}{3}\pi R_{SH}^3$ is the spherical volume and $V_C = \pi R_{CH}^2 \cdot h$ is the cylindrical volume. The spherical hydrodynamic radius is determined from the diffusion constant in water, $D_{water} = \frac{k_B T}{4\pi \cdot \eta_{water} \cdot R_{SH}}$, where η_{water} is the bulk water viscosity. Thus the cylinder height is $h = \frac{4}{3}\frac{R_{SH}^3}{R_{CH}^2}$ and the effective cylinder radius R_{CH} can be found directly from Equation 3 if D_{int} is known.

Taking the experimental values $R_{SH} = 0.6$ nm and $D_{int} = 5.3 \times 10^{-6}$ cm^2/s, we find that $R_{CH} = 1.0$ nm and $h = 0.29$ nm. These dimensions are molecularly plausible (see Figure 9).
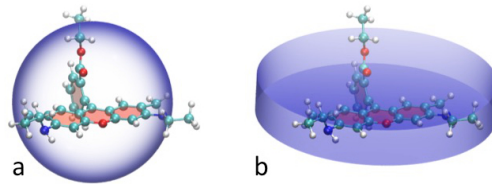
Figure 9: (Color online) Spherical and cylindrical approximation of R6G fluorophore: (a) R6G's hydrodynamic sphere of radius R_{SH}=0.6 nm; (b) R6G's hydrodynamic cylinder of radius R_{CH}=1.0 nm and height h=0.29 nm.

Obtaining accurate values of effective cylindrical radius and height of the R6G would require the exact interfacial viscosity value. This could in principle be determined by comparing the rotational diffusion of some nearly spherical molecule in bulk and at the interface. Such a molecule should be amphiphilic to adsorb at the interface for long times. The choice of such molecule is not obvious.

According to Wang et al. [12], the diffusion coefficients of larger fluorescent tracers, such as the PDI and the larger PDI-based dendrimer, are less affected by the *n*-decane/water interface. The shape of these bulkier, more extended molecules [51] are unlikely to be as affected by the interface; we speculate that they remain closer to spheres, so that the same spherical hydrodynamic approximation is valid for diffusion at both the interface and in the bulk.

Our simulation results, together with a simple model and in comparison with experiments [12], suggest that the restricted orientation of surface-active molecules may significantly affect its diffusion constant, at the oil/water and any other interface. However, these results do not exclude an additional influence from the observed ordering of the bulk phases at the interface, through a reduced or increased surface viscosity. It

would be interesting to test the surface viscosity directly, perhaps with the design of a sufficiently compact and symmetric surface-active molecule for simulation.

Appendix: functions within GROMACS package used in the analysis.

- Self-diffusion coefficient of water was calculated using "g_msd.

- Trajectory of center-of-mass of R6G was extracted using "g_traj.

- Velocity autocorrelation of R6G was calculated using "g_velacc".

- Viscosities were calculated using "g_energy".

- Densities were calculated using "g_density".

- Order parameter of *n*-decane was calculated using "g_order".

- Ordering of water dipoles at the interface was calculated using "g_h2order".

Acknowledgements

References

[1]   Y. Peng, W. Chen, T. M. Fischer, D. a. Weitz, and P. Tong, J. Fluid Mech. **618**, 243 (2008).

[2]   L. Capretto, W. Cheng, M. Hill, and X. Zhang, Top. Curr. Chem. **304**, 27 (2011).

[3]   W. Zhang, S. Chen, N. Li, J. Zhang, and W. Chen, PLoS One **9**, 1 (2014).

[4]   S. Ladha, A. R. Mackie, L. J. Harvey, D. C. Clark, E. J. Lea, M. Brullemans, and H. Duclohier, Biophys. J. **71**, 1364 (1996).

[5]   L. Zhang and S. Granick, Proc. Natl. Acad. Sci. U. S. A. **102**, 9118 (2005).

[6]   S. Ramadurai, A. Holt, V. Krasnikov, G. van den Bogaart, J. A. Killian, and B. Poolman, J. Am. Chem. Soc. **131**, 12650 (2009).

[7]   K. Weiß, A. Neef, Q. Van, S. Kramer, I. Gregor, and J. Enderlein, Biophys. J. **105**, 455 (2013).

[8]   D. Jeong, K. Kim, S. Lee, M. C. Choi, and S. Q. Choi, Langmuir **30**, 14369 (2014).

[9]   M. Negishi, H. Seto, M. Hase, and K. Yoshikawa, Langmuir **24**, 8431 (2008).

[10]   R. B. Walder, A. Honciuc, and D. K. Schwartz, J. Phys. Chem. B **114**, 11484 (2010).

[11]   M. Kastantin, R. Walder, and D. K. Schwartz, Langmuir **28**, 12443 (2012).

[12]   D. Wang, L. Pevzner, C. Li, K. Peneva, C. Y. Li, D. Y. C. Chan, K. Müllen, M. Mezger, K. Koynov, and H. J. Butt, Phys. Rev. E - Stat. Nonlinear, Soft Matter Phys. **87**, 012403 (2013).

[13]   W. L. Jorgensen, D. S. Maxwell, and J. Tirado-Rives, J. Am. Chem. Soc. **118**, 11225 (1996).

[14]   W. L. Jorgensen and J. Tirado-Rives, Proc. Natl. Acad. Sci. U. S. A. **102**, 6665 (2005).

[15]   C. Caleman, P. J. van Maaren, M. Hong, J. S. Hub, L. T. Costa, and D. van der Spoel, J. Chem. Theory Comput. **8**, 61 (2012).

[16]   T. J. Smith, W. Iglesias, E. K. Mann, A. Jákli, and D. J. Lacks, Liq. Cryst. **40**, 159 (2013).

[17]   S. W. I. Siu, K. Pluhackova, and R. A. Böckmann, J. Chem. Theory Comput. **8**, 1459 (2012).

[18]   A. C. Vaiana, A. Schulz, J. Wolfrum, M. Sauer, and J. C. Smith, J. Comput. Chem. **24**, 632 (2003).

[19]   T. Darden, D. York, and L. Pedersen, J. Chem. Phys. **98**, 10089 (1993).

[20]   S. Nosé, J. Chem. Phys. **81**, 511 (1984).

[21] M. Parrinello and A. Rahman, J. Appl. Phys. **52**, 7182 (1981).

[22] D. Van Der Spoel, E. Lindahl, B. Hess, G. Groenhof, A. E. Mark, and H. J. C. Berendsen, J. Comput. Chem. **26**, 1701 (2005).

[23] B. Hess, C. Kutzner, D. van der Spoel, and E. Lindahl, J. Chem. Theory Comput. **4**, 435 (2008).

[24] S. Pronk, S. Páll, R. Schulz, P. Larsson, P. Bjelkmar, R. Apostolov, M. R. Shirts, J. C. Smith, P. M. Kasson, D. van der Spoel, B. Hess, and E. Lindahl, Bioinformatics **29**, 845 (2013).

[25] M. D. Hanwell, D. E. Curtis, D. C. Lonie, T. Vandermeersch, E. Zurek, and G. R. Hutchison, J. Cheminform. **4**, 17 (2012).

[26] J. M. Martínez and L. Martínez, J. Comput. Chem. **24**, 819 (2003).

[27] L. Martínez, R. Andrade, E. G. Birgin, and J. M. Martínez, J. Comput. Chem. **30**, 2157 (2009).

[28] W. Humphrey, A. Dalke, and K. Schulten, J. Mol. Graph. **14**, 33 (1996).

[29] J. Stone, in *Intel Supercomput. Users Gr. Proc.* (1995), pp. 1–5.

[30] D. Milanova, R. D. Chambers, S. S. Bahga, and J. G. Santiago, Electrophoresis **32**, 3286 (2011).

[31] L. Yuan, W. Lin, and Y. Feng, Org. Biomol. Chem. **9**, 1723 (2011).

[32] I.-C. Yeh and G. Hummer, J. Phys. Chem. B **108**, 15873 (2004).

[33] H. J. C. Berendsen, J. R. Grigera, and T. P. Straatsma, J. Phys. Chem. **91**, 6269 (1987).

[34] P. E. Smith and W. F. van Gunsteren, Chem. Phys. Lett. **215**, 315 (1993).

[35] M. Holz, S. R. Heil, and A. Sacco, Phys. Chem. Chem. Phys. **2**, 4740 (2000).

[36] B. Hess, J. Chem. Phys. **116**, 209 (2002).

[37] R. C. Weast, M. J. Astle, and W. H. Beyer, *CRC Handbook of Chemistry and Physics*, 69th ed. (CRC Press, Inc., Boca Raton, Florida, 1988).

[38] C.- Kolmogorov, *Encyclopedia of Statistical Sciences* (John Wiley & Sons, Inc., Hoboken, NJ, USA, 2004).

[39] M. L. McHugh, Biochem. Med. (Zagreb). **18**, 7 (2008).

[40] C. B. Müller, A. Loman, V. Pacheco, F. Koberling, D. Willbold, W. Richtering, and J. Enderlein, EPL (Europhysics Lett. **83**, 46001 (2008).

[41] D. Magde, E. L. Elson, and W. W. Webb, Biopolymers **13**, 29 (1974).

[42] E. W. Lemmon, M. O. McLinden, and D. G. Friend, in *NIST Chem. WebBook, NIST Stand. Ref. Database Number 69*, edited by P. J. Linstrom and W. G. Mallard (National Institute of Standards and Technology, Gaithersburg MD, 20899, 2015).

[43] J. Fraxedas, *Water at Interfaces: A Molecular Approach*, 1st ed. (CRC Press, Boca Raton, Florida, 2014).

[44] W. Norde, *Colloids and Interfaces in Life Sciences* (CRC Press, 2003).

[45] H. Xiao, Z. Zhen, H. Sun, X. Cao, Z. Li, X. Song, X. Cui, and X. Liu, Sci. China Chem. **53**, 945 (2010).

[46] A. R. van Buuren, S. J. Marrink, and H. J. C. Berendsen, J. Phys. Chem. **97**, 9206 (1993).

[47] D. M. Mitrinovic, A. M. Tikhonov, M. Li, Z. Huang, and M. L. Schlossman, Phys. Rev. Lett. **85**, 582 (2000).

[48] B. D. Hughes, B. A. Pailthorpe, and L. R. White, J. Fluid Mech. **110**, 349 (1981).

[49] E. P. Petrov and P. Schwille, Biophys. J. **94**, L41 (2008).

[50] P. G. Saffman, J. Fluid Mech. **73**, 593 (1976).

[51] C. Kohl, T. Weil, J. Qu, and K. Müllen, Chemistry **10**, 5297 (2004).